Experimental investigation of strong-field-ionization theories for laser fields from visible to midinfrared frequencies

Yu Hang Lai, Junliang Xu, Urszula B. Szafruga, Bradford K. Talbert, Xiaowei Gong, Kaikai Zhang, Harald Fuest, Matthias F. Kling, Cosmin I. Blaga, Pierre Agostini, and Louis F. DiMauro

Phys. Rev. A **96**, 063417 — Published 20 December 2017

DOI: 10.1103/PhysRevA.96.063417

Experimental investigation of strong-field-ionization theories for laser fields from visible to mid-infrared frequencies

Yu Hang Lai[1,*], Junliang Xu[1,*], Urszula B. Szafruga[1], Bradford K. Talbert[1], Xiaowei Gong[1], Kaikai Zhang[1], Harald Fuest[2,3], Matthias F. Kling[2,3], Cosmin I. Blaga[1], Pierre Agostini[1] and Louis F. DiMauro[1]
[1] *Department of Physics, The Ohio State University, Columbus, OH 43210, USA*
[2] *Max Planck Institute of Quantum Optics, D-85748 Garching, Germany*
[3] *Physics Department, Ludwig-Maximilians-Universität München, D-85748 Garching, Germany*

Strong field ionization yield versus intensity is investigated for various atomic targets (Ne, Ar, Kr, Xe, Na, K, Zn and Mg) and light polarization from visible to mid-infrared (0.4 - 4μm), from multiphoton to tunneling regimes. The experimental findings (normalized yield *vs* intensity, ratio of circular to linear polarization and saturation intensities) are compared to the theoretical models of Perelomov-Popov-Terent'ev (PPT) and Ammosov-Delone-Krainov (ADK). While PPT is generally satisfactory, ADK validity is found, as expected, to be much more limited.

I. INTRODUCTION

A treatment of strong field atomic ionization (SFI) is essential as the laser intensity approaches an atomic unit of field (50 V/Å). In this regime the electron release time becomes strongly correlated to the extrema of the laser field cycle, at variance with the perturbative description in which electron emission probability is constant over the optical cycle. In addition, the electric force acting on an electron is too strong to be treated as a perturbation: in particular the ionization rate is no longer a power function of the light intensity but an exponential function of the laser field. These crucial properties are at the origin of the success of the semi-classical model[1, 2] which has become the theoretical foundation of many strong-field phenomena such as high-order Above-Threshold Ionization (ATI) plateau [1, 3], non-sequential ionization (NSI) [4], high order harmonic generation (HHG) [5], etc.

Based on early experimental observations, Keldysh [6], more than 50 years ago, conceived the theory that, for low enough frequencies, the photoionization process is similar to a dc-tunneling ionization process. In this picture, the Coulomb potential is "tilted" by the laser field allowing the electron to escape via quantum tunneling through the Stark potential. Thus, the theory simply accounts for both the ionization rate being strongly correlated to the instantaneous field strength of the driving laser and the exponential ionization rate.

Keldysh's approach resulted in a rate expressed as a sum of multiphoton processes, which he expresses as the total ionization rate in Eq.(16) of Ref. [6] as a function of the so-called Keldysh parameter defined as $\gamma = \omega\sqrt{2mI_p}/eF$, which can be interpreted as a ratio of the characteristic atomic momentum $\sqrt{2mI_p}$ to the field induced momentum $p_F = eF/\omega$ [7]. Here I_p is the ionization potential, F and ω the laser field strength and frequency, respectively, and m and e the electron mass and charge, respectively. The rate is a complicated but analytical function of γ which reduces into two simple forms (written here in atomic units for the hydrogen ground state), for $\gamma \ll 1$ (tunneling regime):

$$w_0 = \frac{\sqrt{6\pi}}{4}(\sqrt{I_p}F)^{1/2}\exp\left[-\frac{2(2I_p)^{3/2}}{3F}\left(1-\frac{\gamma^2}{10}\right)\right] \quad (1)$$

and for $\gamma \gg 1$ (multiphoton regime)

$$w_0 \propto \left(\frac{F}{\omega}\right)^{2K_o}, \quad (2)$$

where $K_0 = \lceil I_p/\hbar\omega \rceil$ is the minimum number of photons needed to ionize the atom at low intensity.

An exact form of the pre-exponential factor of the formula for ionization rate in [6] was obtained by Perelomov, Popov and Terent'ev [8, 9], dubbed the PPT formula. The Keldysh rate (as well as PPT) depend on two parameters, γ and K_0. These theories are for short range potentials (an essential condition) and a weak laser field ($F \ll 1$ at. un.) for the H ground state, but are valid for all values of γ and wavelengths [7]. A first-order correction was later introduced to account for the long range Coulomb interaction [10, 11].

It is only after the first quantitative experimental evidence of a non-perturbative ionization by a CO_2 laser [12], that the Keldysh theory gained momentum. Subsequently a simplified version was introduced by Ammosov, Delone and Krainov (ADK) [13–15]. The ADK rate can easily be obtained from PPT by taking the limit $\gamma \to 0$ and therefore its validity is more limited. One of the overall limitations of tunneling theories is that if the small values of γ are realized by increasing the intensity at constant wavelength, the concept of tunneling becomes meaningless since the cusp of the Stark potential becomes lower than the atomic ground state energy [14, 16]. It happens when the laser intensity is higher than the so-called barrier-suppression ionization (BSI) intensity $I_{BSI} = I_p^4/16$ (in atomic units).

Attempts have been made to extend tunnel ionization theory to the BSI regime [15, 17–19]. Other SFI theories without reference to tunneling were proposed by Faisal [20] and, based on S-matrix formulation and radiation gauge, by Reiss [21]. (For a review, see [7]). In addition, ab initio simulations using numerical solutions

of the time-dependent Schrödinger equation (TDSE) became available in the late 1980s [22–24]. Certainly the analytical theories, compared to experiment, led to much easier computations, in addition to their closed forms.

Until the mid-1970s, studying SFI was not experimentally accessible due mainly to the "long" laser pulse technology ($\geq$ 100 ps) which limited the effective intensity experienced by the atom due to ground state depletion. Although some hint of possible non-perturbative extension of ionization to ATI was reported[25] it really took measurements with a CO_2 laser [12] to convince the community of the reality of exponential rates. As intense, near-infrared femtosecond laser pulses became widely available, a rich set of strong field phenomena were observed and explored, and many ultrafast techniques have emerged, such as stereo ATI measurement of the carrier-to-envelope phase (CEP) [26, 27], attosecond pulse generation [28–30], laser-induced electron diffraction [31–34], etc.

SFI yields as a function of laser intensity have been investigated mainly for noble gas atoms using near-infrared (NIR) wavelengths ($\leq$ 1 μm). Ion yields measurements on alkali and alkaline earth atoms have also been studied in the multiphoton regime [35–38], but no comparison with SFI theories were made. Saturation intensities (relative to xenon) in transition metals have been compared to ADK predictions with strong disagreement factors ranging from 2 to 7[39]. Similar SFI comparisons for organic molecules have resulted in similar disagreement with ADK [40]. The only case of a single electron atom (H) ionization [41, 42] concluded in excellent agreement with TDSE but was not compared to the SFI theories. A comparison of SFI theories with TDSE can be found in [18] for the BSI regime and in recent papers [43, 44].

In practical application ADK is more commonly used than PPT due to its simplicity. It has been widely used even in the regime of $\gamma \sim 1$. In the present paper, we aim to investigate the applicability of PPT and ADK by a comprehensive comparative study between experiment and theories of the total intensity-dependent ionization yield for different atom species at different laser wavelengths at linear and circular polarizations. Ion yield measurements are performed on atomic targets including noble gases (Ne, Ar, Kr, Xe), alkali (Na, K), alkaline earth (Mg) and one transition metal (Zn) with wavelengths ranging from 0.4 to 4 μm. γ is ranging from 0.2 to 8.3. By comparing the relative yields to the PPT and ADK analytical probabilities we evaluate the theories and in particular, the applicability of ADK formula which is in principle limited to the deep tunneling regime. Since we do not perform absolute measurements, the signal versus intensity is freely normalized to the theory, for example on the highest intensity point. The intensity dependence can be then compared to the theoretical ones. Moreover, comparisons were made using the quantities which are independent of the absolute yields including the derivative of log(Ion Yield) with respect to I which has a unit of I^{-1}; the saturation intensities, and the ion yields ratio of linearly and circularly polarized driving fields at a fixed intensity.

II. EXPERIMENT

Our studies use two titanium sapphire laser systems (0.8 μm central wavelength) delivering 80-100 fs pulses with a maximum energy of 12 mJ at 1 kHz repetition rate. These systems pump different optical parametric amplifiers (OPA) providing tuning over $1-2$ μm and $3-4$ μm. The laser pulse energy is controlled by a half-wave plate followed by a polarizer, complemented by neutral density filters or pellicle beamspliters. Ellipticity is controlled by the quarter wave plate mounted after these optics. The pulses are focused into the chamber by a lens with a focal length of 100 mm. The noble gases are delivered with a constant flow rate into the vacuum chamber through a leak valve. The metal targets are prepared by heating the sample in an effusive source oven mounted below the interaction region. Laser intensities were calibrated by the $10U_p$ cutoff in photoelectron spectrum of noble gases [31, 45, 46]. The experimental intensities in some cases are slightly scaled ($\leq$ 20% from the calibration) to achieve best fit to the theoretical ion yield curves. To switch between linear and circular polarization (LP and CP) at a fixed intensity, the QWP is rotated without adjusting the laser energy (that the CP field is the LP field $/\sqrt{2}$).

All the ion yields measurements were performed using a 0.5 m long home-built Wiley-McLaren time-of-flight spectrometer [47]. Ions are extracted and accelerated by a static electric field and collected at the end of the field-free flight tube by a microchannel-plate (MCP) chevron detector. The signal is amplified, discriminated and recorded by a time-to-digital converter with a 1 ns resolution. Each data point is normalized to the number of laser shots and the gas density. The number of laser shots for a data point is at least 6×10^4. The base pressure of the chamber is around 10^{-9} torr. The background ion counts are mainly from water which is mass resolved from the atom targets.

Table I summaries the driving wavelengths and intensity range in the experiments of different target atoms.

III. RESULTS

We first present the results of noble gas atoms, which are the most commonly used targets in strong field studies. The ion yields as a function of laser intensity for Xe, Kr, Ar and Ne at different wavelengths (see captions) are displayed in Figs. 1 to 4. The symbols are experimental data and the full and dashed curves are the PPT and ADK calculations, respectively. In general, for both LP and CP cases, the yields increase rapidly at low intensities and progressively saturate. Beyond saturation

TABLE I. Driving wavelengths λ and intensities ranges ($I_{min} - I_{max}$) of experimental data. The uncertainty of our intensity calibration is about 20%. The γ value at the barrier-suppression intensity I_{BSI} and I_{min} are denoted as γ_{BSI} and γ_{max} respectively.

	λ (μm)	I_{min} (TW/cm^2)	I_{max} (TW/cm^2)	γ_{BSI}	γ_{max}
Ne	0.8	114	1030	0.46	1.3
Ar	0.4	26	240	1.5	4.5
	0.8	24	390	0.73	2.3
	1.3	58	230	0.45	0.91
Kr	0.8	16	200	0.88	2.7
	3.3	26	140	0.21	0.52
	3.6	30	130	0.19	0.44
	3.9	29	100	0.18	0.41
Xe	0.8	11	170	1.1	3
	3.3	21	89	0.26	0.54
Zn	0.8	21	110	1.6	1.9
	1.3	35	150	0.98	0.92
	2	23	120	0.64	0.74
	3.6	21	120	0.35	0.43
Mg	0.4	3.7	75	4.4	8.3
	0.8	6.1	52	2.2	3.2
	3.6	9.7	44	0.49	0.57
Na	3.2	1.9	10	0.98	1.2
	3.6	2	11	0.87	1
	3.7	2.2	9.1	0.85	0.95
	4	1.9	12	0.79	0.94
K	3.2	0.83	5.8	1.3	1.7
	3.6	0.66	4.8	1.1	1.7
	4	0.71	4.7	1	1.4

the yield follows a $I^{3/2}$ scaling due to the geometrically expanding Gaussian focal volume [48].

The lower ionization potentials of alkali atoms relative to noble gases require a significantly lower laser intensity to avoid saturation. Thus, longer wavelengths (mid-infrared [MIR]) are used to achieve comparable γ values to the noble gases. Ionization yields as a function of intensity for Na atoms at 3.6 μm are shown in Fig. 5. Similar to the noble gases in NIR, the ionization yields increase rapidly with intensity and eventually approach the $I^{3/2}$ scaling. Other curves for Na and K for linearly polarized light at different MIR wavelengths are shown in Fig. 6.

Ion yields curves of transition metal Zn at 3.6, 2, 1.3 and 0.8 μm are displayed in Fig. 7. Figure 8 shows the results of Mg at 3.6 and 0.8 μm.

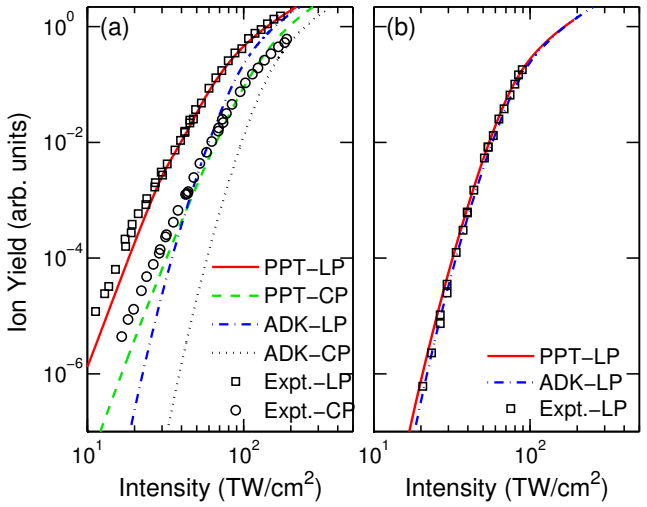

FIG. 1. (Color online) Ion yields of Xe as a function of intensity at (a) 0.8 μm and (b) 3.3 μm. LP:linear polarization; CP:circular polarization

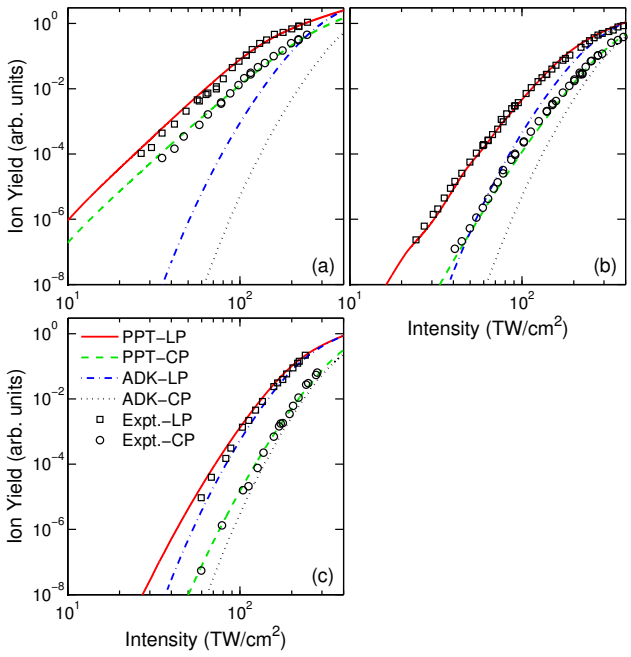

FIG. 2. (Color online) Ion yields of Ar as a function of intensity at (a) 0.4 μm, (b) 0.8 μm and (c) 1.3 μm for linear and circular polarization.

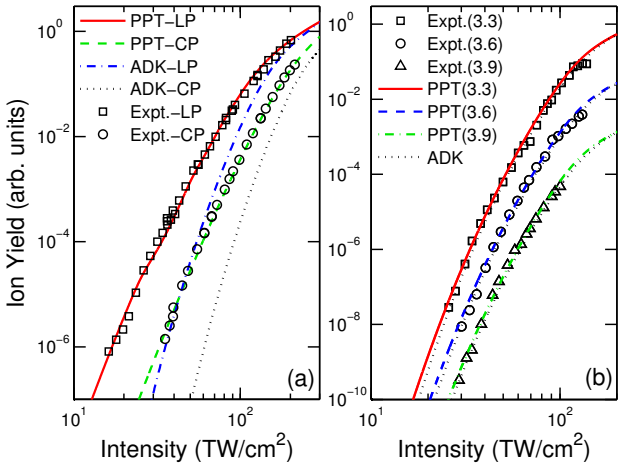

FIG. 3. (Color online) Ion yield of Kr as a function of intensity at (a) 0.8 μm and (b) 3.3, 3.6 and 3.9 μm. The three data sets are displaced from each other arbitrarily along the vertical axis for clear illustration.

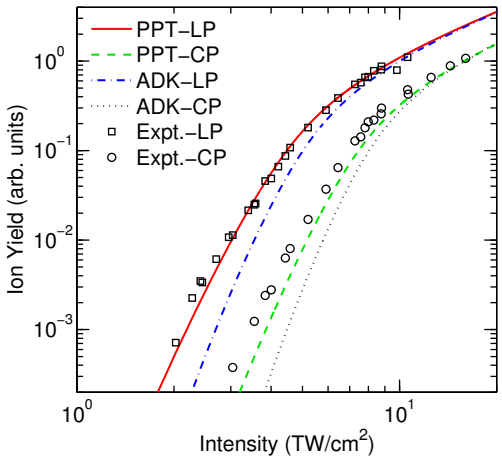

FIG. 5. (Color online) Ion yield of Na as a function of intensity at 3.6 μm.

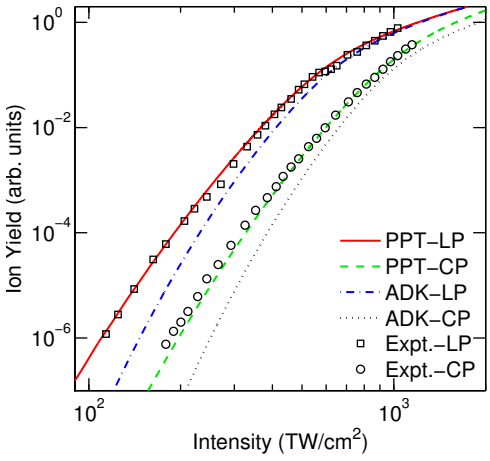

FIG. 4. (Color online) Ion yields of Ne as a function of intensity at 0.8 μm.

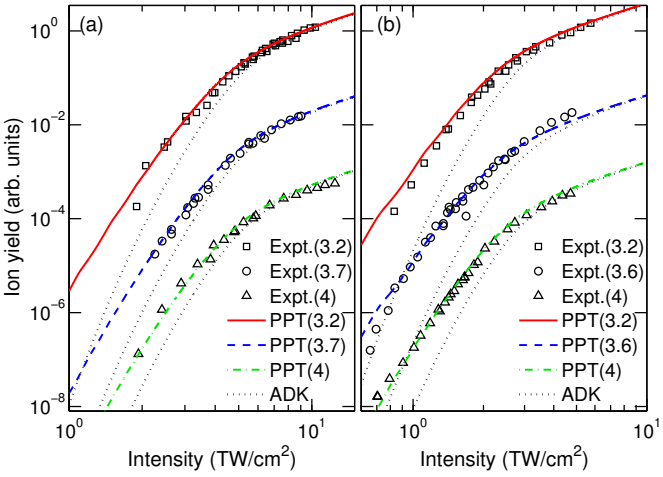

FIG. 6. (Color online) Ion yields as a function of intensity of (a) Na at 3.2, 3.7 and 4 μm; (b) K at 3.2, 3.6 and 4 μm. The three data sets in each panel are displaced from each other arbitrarily along the vertical axis for clear illustrations.

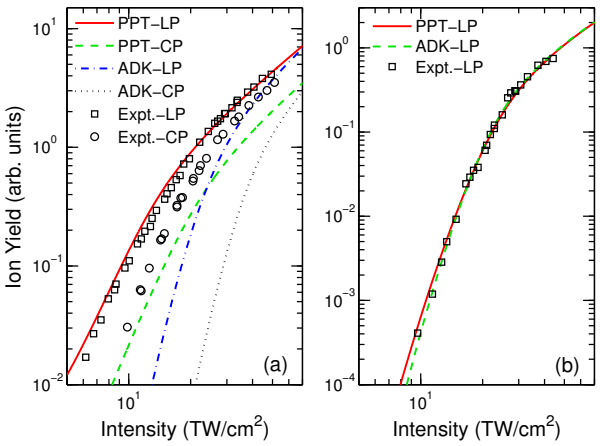

FIG. 7. (Color online) Ion yields of Zn as a function of intensity at (a) 3.6 μm, (b) 2 μm, (c) 1.3 μm, and (d) 0.8 μm.

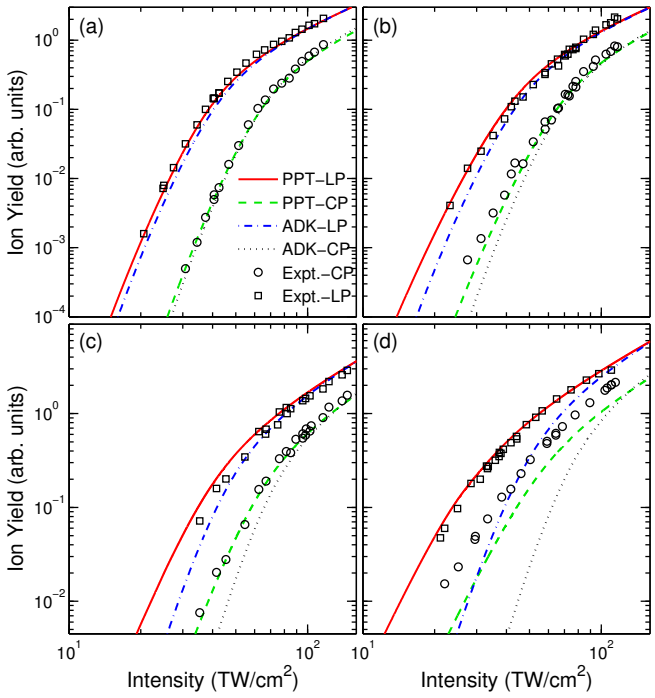

FIG. 8. (Color online) Ion yields of Mg as a function of intensity at (a) 3.6 μm and (b) 0.8 μm.

IV. DISCUSSION

We begin the discussion with Xe, a common benchmark in SFI. Figure 3 shows Xe ionized at 3.3 and 0.8 μm. For 3.3 μm γ-parameter ranges from about 0.2 to 0.5 and both PPT and ADK results are close to each other and agree with the measurement. At 0.8μm, PPT and experiment still agree but ADK predicts a much more rapid intensity dependence. Qualitatively, similar conclusions regarding the comparison between experiments and theories can be drawn from other target atoms such as Ar (Fig.2), Kr (Fig.3), Zn (Fig.7) and Mg (Fig.8). Overall, these results confirm the validity of ADK at small γ and the superiority of PPT for all cases.

In the following three subsections, we will present absolute comparisons between experiments and theories using the following three quantities which do not require absolute measurements of ionization probabilities. The first is $Y_d \equiv d(log(Y))/dI$ which is the derivative of log(Ion Yield) with respect to laser intensity I and has units of I^{-1}. Note that Y_d is also equivalent to $(1/Y)dY/dI$ which is the slope of the ion yield divided by the yield. The second quantity is the saturation intensity I_{sat} and the last is a dimensionless quantity $R \equiv Y_{CP}/Y_{LP}$ which is the ion yield ratio between CP and LP.

A. Intensity dependence of ion yields

To compute Y_d from discrete experimental data points, a polynomial fit to the data ($\log_{10}$(Ion yield) vs intensity) is performed (see caption of Fig. 9) from which the derivative is extracted. The data of Xe at 0.8 μm and the fitted curve are shown in Fig. 9(a). The values of Y_d calculated from the fitted curve and the theoretical curves are displayed in Fig. 9(b). It can be seen that PPT and experiment are in excellent agreement while ADK overestimates. Note that the modulation on the PPT curve is due to channel closures (condition $I_p + U_p = n\hbar\omega$). The same procedure is applied to other data sets and the results are compiled in Fig. 10, which shows the ratio between theoretical (PPT and ADK) and experimental values of Y_d at an intensity of $0.8I_{BSI}$. Here γ ranges from 0.2 to 2.4. Note that the closer the ratio is to one, the better is the agreement between theory and experiment. In the comparison between experiments and PPT, the ratio is close to one (ranging between 0.9 and 1.2) in all the data set, even when γ is greater than 2. For ADK, good agreement with experiments is observed for small γ values but as it approaches 1 the deviation becomes significant.

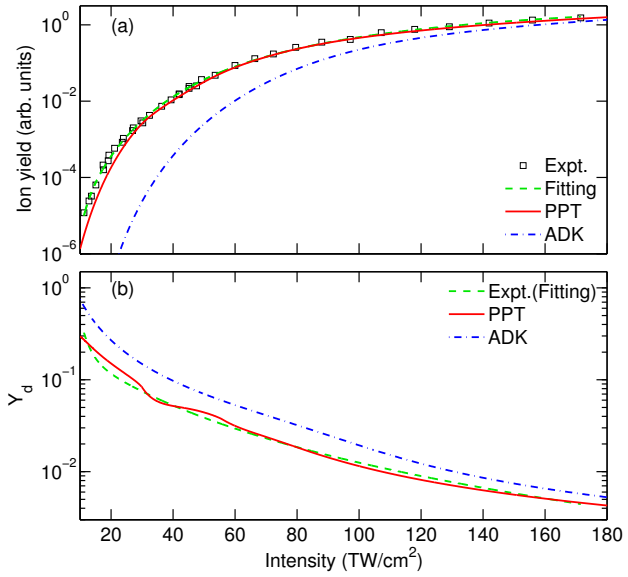

FIG. 9. (Color online) (a) log(Ion yield) of Xe as a function of intensity at 0.8 μm. The fitting function is a polynomial of $1/F$ up to the fifth order, where F is the field amplitude. The fitting parameters are the coefficients of the polynomial. (b) $d(log(Y))/dI$ calculated from the fitted curve (green dashed line), PPT (red solid line) and ADK (blue dash-dot line) calculations.

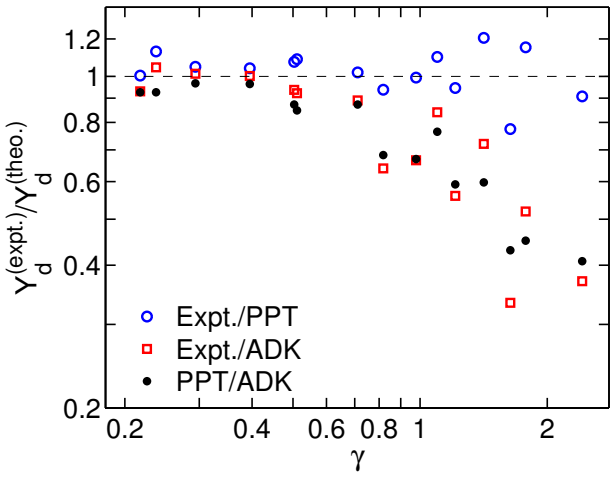

FIG. 10. (Color online) The ratio between theoretical (PPT and ADK) and experimental values of Y_d at an intensity of $0.8I_{BSI}$ for different data set. From left to right: Kr (3.6 μm), Kr (3.3 μm), Xe (3.3 μm), Zn (3.6 μm), Ar (1.3 μm), Ne (0.8 μm), Zn (2 μm), Ar (0.8 μm), Kr (0.8 μm), Na (3.2 μm), Xe (0.8 μm), K (3.2 μm), Ar (0.4 μm), Zn (0.8 μm) and Mg (0.8 μm).

B. Saturation intensity

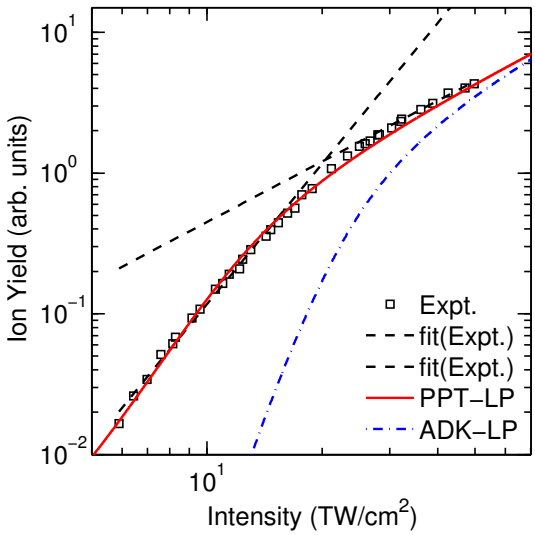

FIG. 11. (Color online) Ion yields of Mg at 0.8 μm. Saturation intensity obtained from experimental data, PPT and ADK calculations are given by the intersection point of the two fitting (black dashed) lines.

Figure 11 shows ion yields of magnesium of 0.8 μm. The two black dashed lines are two linear fits to the data, one is fitted to the data points at low intensities and the other one is fitted to the data points beyond the saturation intensity which should have a slope close to 1.5. Here I_{sat} is defined to be the intersection of the two linear fits. For this data set I_{sat} is determined to be 20 TW/cm^2. The same fitting procedures are applied to the ADK and PPT curves to obtain the theoretical predictions of I_{sat}, the values obtained from ADK and PPT are 29 TW/cm^2 and 18 TW/cm^2 respectively.

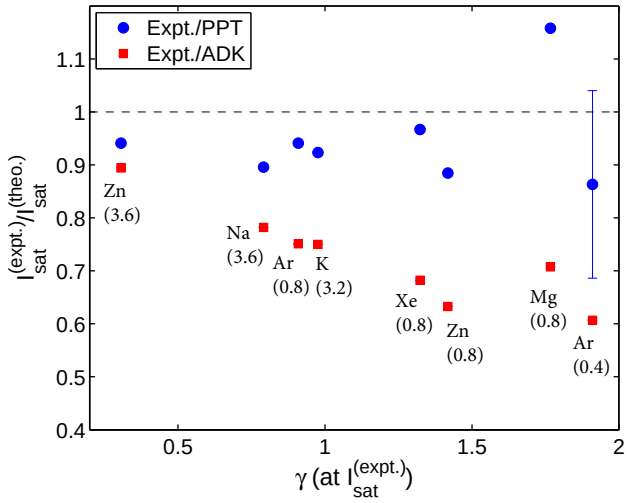

FIG. 12. (Color online) The ratio between measured and theoretically predicted (PPT and ADK) values of saturation intensities for various targets and driving wavelengths. γ are calculated using the experimental values of saturation intensities. Each point has an error bar of 20% in intensity due to the uncertainty in intensity calibrations. The bracketed numbers under the atomic symbol represents the driving wavelength (in μm).

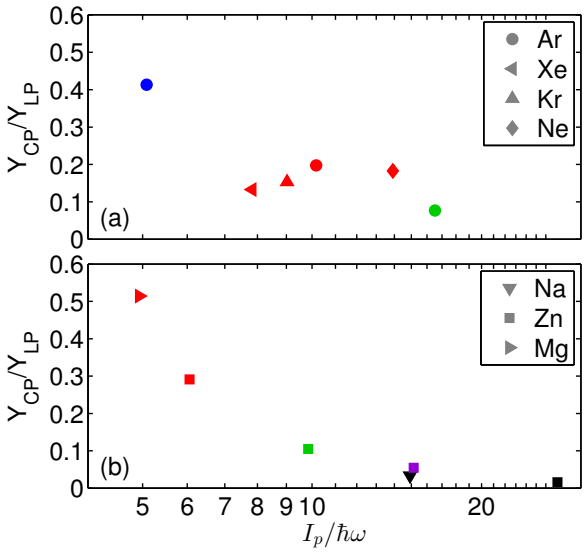

FIG. 13. (Color online) The ion yield ratio between CP and LP at different target atoms and wavelengths. Laser intensity is at I_{BSI}. Panel (a) shows the results for noble gases, from left to right: Ar (0.4 μm), Xe (0.8 μm), Kr (0.8 μm), Ar (0.8 μm), Ne (0.8 μm) and Ar (1.3 μm). Panel (b) shows the results for metal atoms, from left to right: Mg (0.8 μm), Zn (0.8 μm), Zn (1.3 μm), Na (3.6 μm), Zn (2 μm) and Zn (3.6 μm). Blue: 0.4 μm; red: 0.8 μm; green: 1.3 μm; purple: 2 μm; black: 3.6 μm.

I_{sat} for different data set were obtained using the same method and the results are summarized in Fig. 12. It shows the ratio between the measured and theoretically predicted I_{sat} for various targets and driving wavelengths. Overall, PPT agrees well with experiments within 20% uncertainty. Except for small γ, in general ADK overestimates I_{sat} and the deviation increases with γ. Note that there is an ambiguity in the determination of I_{sat} using the fitting method described above since the slope of the low intensity part of an ion yield curve varies as a function of intensity. However, since the y-range for the fittings to the experimental and theoretical results are set to be the same, the ratio between the fitted I_{sat} from the two curves indeed represents a real deviation between them.

C. Linear vs circular polarization

CP and LP lead to very different ATI energy spectra [3, 21, 49] due to the fact that in CP the photoelectron classical motion never returns to the parent ion. Differences are also expected in the total ionization rates w_c and w_l. While in the tunneling regime, for small γ, w_l is usually larger than w_c, the opposite can be true in the multiphoton domain[50]. PPT [8] predicts rate ratio CP/LP < 1, depending on the field strength.

Turning to the experiment, the ratio CP/LP is an interesting quantity which does not imply absolute comparisons. Fig. 7 shows the results of Zn and Fig. 2 shows the results of Ar at different wavelengths for both polarizations. One general feature is that the yield at LP is larger than the yield at CP at the same laser intensity and the difference increases as the photon energy decreases. Fig. 13 shows the ratio R of different target atoms at different wavelengths and it can be observed that the ratio decreases as $I_p/\hbar\omega$ increases. In the tunneling regime, it is expected that the yield at LP is much larger than the yield at CP because peak amplitude of the field for LP is a factor of $\sqrt{2}$ larger than that for CP when the intensity is fixed.

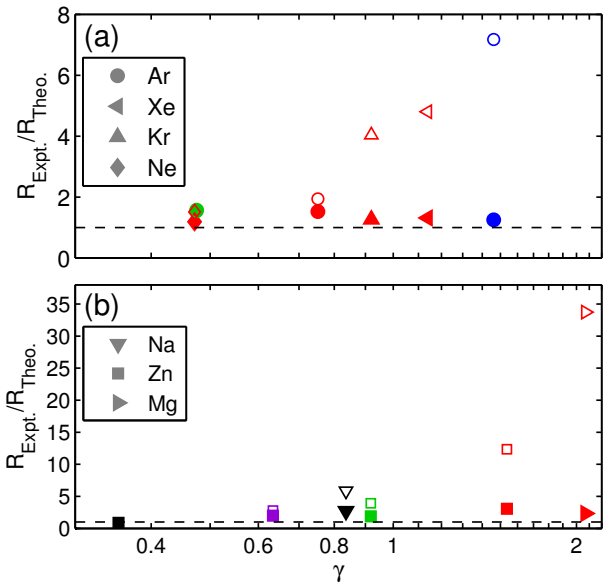

FIG. 14. (Color online) The ratio between theoretical (PPT and ADK) and experimental values of $R \equiv Y_{CP}/Y_{LP}$. Laser intensity is at I_{BSI}. R_{Expt} is the experimental value of R and R_{Theo}. is the theoretical value of R The filled symbols are the ratio between PPT and experiment and the open symbols are the ratio betten ADK and experiment. Panel (a) shows the results for noble gases, from left to right: Ne (0.8 μm), Ar (1.3 μm), Ar (0.8 μm), Kr (0.8 μm), Xe (0.8 μm) and Ar (0.4 μm). Note that the data points of Ne (0.8 μm)and Ar (1.3 μm) are very close to each other. Panel (b) shows the results for metal atoms, from left to right: Zn (3.6 μm), Zn (2 μm), Na (3.6 μm), Zn (1.3 μm), Zn (2 μm) and Mg (0.8μm),. Blue: 0.4μm; red: 0.8μm; green: 1.3 μm; purple: 2 μm; black: 3.6 μm.

To quantify the deviations between experimental results with PPT and ADK, we take the ratio between experimental and calculated (from PPT or ADK) values of R for different data sets and the results are plotted as a function of γ in Fig. 14. All the comparisons are performed approximately at the calculated values of over-the-barrier intensities. Again, the closer the ratio to one, the better the agreement between experiment and theory. The experiment to PPT ratio is ranging between 0.8 and 3 and does not show a significant trend of increase as a function of γ. The experiment to ADK ratio is close to that of PPT for small γ values, but as γ approaches 1 the ratio start to increase significantly and in the multiphoton regime ADK predictions become an order of magnitude larger than the experimental results.

D. Few-photon ionization in large γ regime

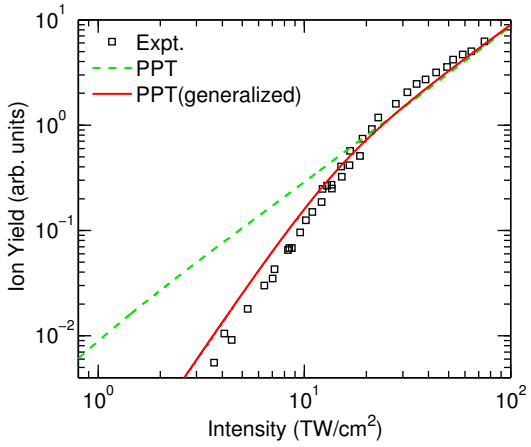

FIG. 15. (Color online) Ion yields of Mg as a function of intensity at 0.4 μm. Squares: Experimental data. The experimental intensities are scaled using the saturation intensity obtained from the TDSE calculations in [51] as a benchmark. Green dashed line: PPT calculations with original version of Coulomb correction factor (Eq. (4)). Red solid line: PPT calculations with generalized version of Coulomb correction factor (see text). For visibility, the blue curve is multiplied by 0.01 relative to the red curve.

While the data presented in previous sections have demonstrated that PPT formula (Eq. (3)) works well in both multiphoton and tunneling regime, we would like to point out that there is a limit on γ for Eq. (3) to be valid. It is due to the fact that the Coulomb correction (CC) factor $(2/Fn^{*3})^{2n*}$ (see Appendix) was derived under the assumption that $\gamma \ll 2I_p/\sqrt{F}$ [10].

Figure 15 shows ion yields of Mg at 0.4 μm. In this case $\gamma > 2I_p/\sqrt{F}$ for all the data points. Below saturation, the intensity dependence of the data is $\sim I^3$, as predicted by perturbation theory and consistent with the TDSE results in [51]. However, the PPT calculations (green dashed line in Fig. 15) shows that the ionization probability saturates at an intensity much lower than the intensity range of Fig. 15, so the slope of the curve is just 3/2 due to the expanding focal volume, and even at very low intensities it remains much smaller than 3. It should be pointed out, that although the short-range potential (with no CC) PPT does predict a power law $\sim I^{K_0}$, in agreement with perturbation theory (see Eq. (2.4) in [9]) in the large γ limit (this results of the Keldysh function [6] and is confirmed by our PPT calculation), it cannot predict the correct ionization rate. In many cases, it over estimates the saturation intensities by an order of magnitude or more. Popruzhenko *et al.* [11] derived a new expression of the CC factor of PPT formula, $(2/Fn^{*3})^{2n*}(1+2\gamma/e)^{-2n*}$, valid for arbitrary values of γ. With this generalized version of CC factor, good agreement between experiment and PPT calcula-

tions (red solid curve in Figure 15) is obtained. For clarification, PPT calculations with CC factor $(2/Fn^{*3})^{2n*}$ (Eq. 4), without CC factor and with generalized CC factor $(2/Fn^{*3})^{2n*}(1+2\gamma/e)^{-2n*}$ are displayed in Fig. 16.

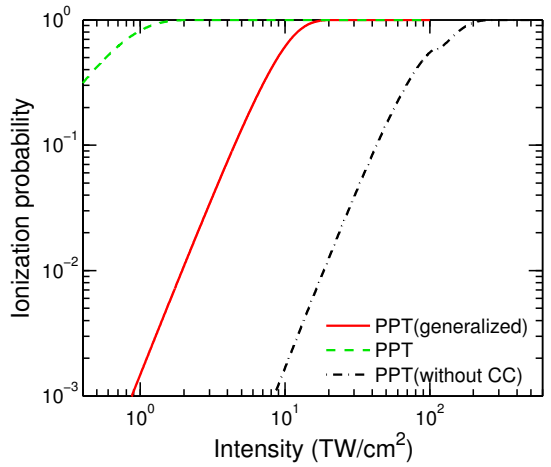

FIG. 16. (Color online) Calculated ionization probability of Mg at 0.4 μm using PPT without CC factor (black dash-dot line); with CC factor $(2/Fn^{*3})^{2n*}$ (green dashed line); and with generalized CC factor $(2/Fn^{*3})^{2n*}(1+2\gamma/e)^{-2n*}$ (red solid line). Effect of focal volume averaging is not taken into account. For both solid and dashed lines the slopes are close to K_0, but the saturation intensity is different by an order of magnitude.

V. SUMMARY

We have presented an experimental study on ionization of atoms in intense laser fields at different wavelengths, intensities, polarizations and types of targets with the goal of evaluating PPT and ADK models. Our data covers a wide range of γ values. In particular, we carried out the first experiment on tunnel ionization of alkali and alkaline earth atoms in the mid-infrared as a test of the applicability of Keldysh metric in atoms with very low ionization potentials. The PPT model agrees well with all the experimental data presented in this paper but must include a generalized Coulomb correction factor [11] in the very large γ regime in which ionization is a few-photon process. The ADK model significantly underestimates the ionization yield except in the deep tunneling regime. PPT also gives much better predictions for ionization yield ratio between CP and LP than ADK. ADK underestimates the CP/LP ratio by an order of magnitude when γ is large (approaches 2).

ADK has also been extended to molecules in a version called MO-ADK [52]. However, MO-ADK failing to give an accurate prediction on the orientation-dependent ionization profile for simple molecules CO_2 [53, 54] (and also polar molecules CO [55, 56]) with $\gamma > 1$ has caused a long debate. More elaborate models [57–63] have been attempted with various correction schemes. However, the fact that MO-ADK or ADK is supposes to be valid only in the regime of $\gamma \ll 1$, a criterion which is not met in the aforementioned studies, should not be overlooked. Recently, PPT formula has also been generalized to molecules by Zhao et al[44].

VI. ACKNOWLEDGMENTS

This material is based upon work supported by the National Science Foundation under Grant No. 1605042. DiMauro group acknowledges the support of Ohio Supercomputer Center (Project No. PAS0207). HF and MFK acknowledge support from the EU via the ERC grant ATTOCO and from the DFG via the excellence cluster "Munich Centre for Advanced Photonics".

VII. APPENDIX: PPT *vs* ADK

For convenience, the basic analytical formulas of the theories are recalled here. For details and derivations the reader is referred to the original papers.

The PPT ionization rate formula is expressed as:

$$w_{PPT}(F,\omega) = \sum_{q\geq q_{min}}^{\infty} w_q(F,\omega), \tag{3}$$

where F and ω are the amplitude and frequency of the laser field, respectively. The partial rates w_q can be interpreted as the ATI rates corresponding to q-photon ATI with q running from a minimum value $q_{min} \equiv \lceil (I_p+U_p)/\omega \rceil$, the minimum number of photons required to reach the effective ionization threshold I_p+U_p to infinity. The full cycle-averaged PPT expression is [8]:

$$\begin{aligned} w_{PPT}(F,\omega) =& c^2_{n^*l^*} f(l,m) I_p \left(\frac{2}{Fn^{*3}}\right)^{2n^*-|m|-1} \\ & \times (1+\gamma^2)^{|m|/2+3/4} A_m(\omega,\gamma) \\ & \times \exp\left[-\frac{2(2I_p)^{3/2}}{3F} g(\gamma)\right], \end{aligned} \tag{4}$$

with

$$g(\gamma) = \frac{3}{2\gamma}\left[\left(1+\frac{1}{2\gamma^2}\right)\sinh^{-1}\gamma - \frac{\sqrt{1+\gamma^2}}{2\gamma}\right],$$

$$\begin{aligned} A_m(F,\omega) =& \frac{4\gamma^2}{\sqrt{3\pi}|m|!(1+\gamma^2)} \\ & \times \sum_{q\geq q_{min}}^{\infty} e^{-\alpha(\gamma)(q-\nu)} w_m\left(\sqrt{\beta(\gamma)(q-q_{min})}\right), \end{aligned}$$

$$w_m(x) = \frac{x^{2|m|+1}}{2}\int_0^1 \frac{e^{-x^2 t} t^{|m|}}{\sqrt{1-t}} dt,$$

$$\alpha(\gamma) = 2\left(\sinh^{-1}\gamma - \frac{\gamma}{\sqrt{1+\gamma^2}}\right),$$

$$\beta(\gamma) = \frac{2\gamma}{\sqrt{1+\gamma^2}},$$

$$\nu = \frac{I_p}{\omega}\left(1+\frac{1}{2\gamma^2}\right),$$

where $c^2_{n^*l^*} = \dfrac{2^{2n^*}}{n^*\Gamma(n^8+l^*+1)\Gamma(n^*-l^*)}$ and $f(l,m) = \dfrac{(2l+1)(l+|m|)!}{2^{|m|}(|m|)!(l-|m|)!}$. In above equations, F is the field amplitude, $n^* = 1/\sqrt{2I_p}$ is the effective quantum number, $l^* = n^* - 1$ is the effective orbital quantum number, $\Gamma(x)$ is the gamma function, and l and m are orbital and magnetic quantum numbers, respectively, with respect to the quantization axis defined by the laser polarization direction. The factor $(2/Fn^{*3})^{2n^*}$ in Eq. (4) takes long range Coulomb interaction into account and $\sqrt{3Fn^{*3}/\pi}$ is the result due to cycle averaging. It is known that the $m = 0$ orbital dominates the ionization as its electron density is primarily distributed along the quantization axis, where all nonzero m orbitals exhibit nodes which doesn't favor ionization of the electron.

For circular polarization, the cycle-averaged PPT rates are given by [64]

$$\begin{aligned} w^s_{PPT}(F,\omega) =& \frac{c^2_{n^*l^*}I_p}{4\sqrt{2\pi}q^{3/2}_{min}}\left(\frac{2}{Fn^{*3}}\right)^{2n^*}(1+\frac{1}{\gamma^2})^{1/2} \\ &\times \sum_{q\geq q_{min}}^{\infty}(1+\zeta)\sqrt{1-\zeta}\left(\frac{1+\gamma^2}{\zeta^2+\gamma^2}\right)^{3/4} \\ &\times e^{-\frac{4q_{min}}{1+\zeta}\left(\tanh^{-1}\sqrt{\frac{\zeta^2+\gamma^2}{1+\gamma^2}}-\frac{\zeta^2+\gamma^2}{1+\gamma^2}\right)}, \end{aligned} \tag{5}$$

for s orbitals,

$$\begin{aligned} w^{p_0}_{PPT}(F,\omega) =& \frac{3c^2_{n^*l^*}I_p}{16\sqrt{2\pi}q^{5/2}_{min}}\left(\frac{2}{Fn^{*3}}\right)^{2n^*}\left(1+\frac{1}{\gamma^2}\right)^{3/2} \\ &\times \sum_{q\geq q_{min}}^{\infty}(1-\zeta^2)\sqrt{1-\zeta} \\ &\times \left(\frac{1+\gamma^2}{\zeta^2+\gamma^2}\right)^{5/4} \\ &\times e^{-\frac{4q_{min}}{1+\zeta}\left(\tanh^{-1}\sqrt{\frac{\zeta^2+\gamma^2}{1+\gamma^2}}-\frac{\zeta^2+\gamma^2}{1+\gamma^2}\right)}, \end{aligned} \tag{6}$$

for p orbitals with $m = 0$, and

$$\begin{aligned} w^{p\pm}_{PPT}(F,\omega) =& \frac{3c^2_{n^*l^*}I_p}{8\sqrt{2\pi}q^{3/2}_{min}}\left(\frac{2}{Fn^{*3}}\right)^{2n^*}\left(1+\frac{1}{\gamma^2}\right)^{3/2} \\ &\times \sum_{q\geq q_{min}}^{\infty}\left(\sqrt{\frac{\zeta^2+\gamma^2}{1+\gamma^2}}\mp\zeta\,\mathrm{sign}(m)\right)^2 \\ &\times \frac{1}{\sqrt{1-\zeta}}\left(\frac{1+\gamma^2}{\zeta^2+\gamma^2}\right)^{3/4} \\ &\times e^{-\frac{4q_{min}}{1+\zeta}\left(\tanh^{-1}\sqrt{\frac{\zeta^2+\gamma^2}{1+\gamma^2}}-\frac{\zeta^2+\gamma^2}{1+\gamma^2}\right)}, \end{aligned} \tag{7}$$

for p orbitals with $m = \pm 1$. Note that $q_{min} = (2U_p + I_p)/\omega$ for circular polarization and $\zeta \equiv 2q_{min}/q - 1$. Eq. (5) and (7) are Eq. (88) and (90) in [64] multiplied by the Coulomb correction factor $(2/Fn^{*3})^{2n^*}$ [10].

The ionization rate for $m = 0$ states is much smaller than the rate for $m = \pm 1$ states. In our calculations for ionization probability, contributions from $m = \pm 1$ states are summed and $m = 0$ state is neglected.

The Ammosov-Delone-Krainov (ADK) ionization rate, on the other hand, is given by

$$\begin{aligned} w_{ADK}(F) =& c^2_{n^*l^*}f(l,m)I_p\left(\frac{2}{Fn^{*3}}\right)^{2n^*-|m|-1} \\ &\times e^{-2(2I_p)^{3/2}/3F}. \end{aligned} \tag{8}$$

This ADK formula for instantaneous ionization rate can be derived from eqn.(4) by taking the limit $\gamma \to 0$ (physically, this corresponds to ionization in a static electric field) and dropping the prefactor due to cycle averaging. Since the ADK formula does not contain ω, it is not able to predict any wavelength dependence of ionization rates. Since it is applied for calculating instantaneous rate, both CP and LP take the same formula and ionization rate is dominated by $m = 0$. It should be stressed that no discrete binding states other than the ground state are considered in PPT or ADK which, as Keldysh or more generally KFR theories, are in principle limited to short range potentials (e.g. in photo-detachment). The atomic parameters required for the calculations presented in this paper are tabulated in Table II.

Ionization probability by a laser pulse is given by

$$P = 1 - e^{-\int_{-\infty}^{+\infty} w(F_0(t))dt}, \tag{9}$$

where $F_0(t)$ is the pulse envelope which is assumed to have a sine-squared shape with pulse durations (FWHM in intensity). In our experiments the ions emerge from the full Gaussian laser beam focus, so 3D volume averaging is applied to the calculations. That is, the total yield is the sum of the yields at each laser intensity, weighted by the corresponding volume element [65].

TABLE II. Atomic parameters.

	I_p (eV)	n^*	$c^2_{n^*l^*}$	I_{BSI} (TW/cm^2)
Ne	21.56	0.794	4.244	862
Ar	15.79	0.929	4.116	246
Kr	13.99	0.986	4.025	153
Xe	12.13	1.059	3.882	86
Na	5.14	1.627	2.290	2.8
K	4.34	1.770	1.890	1.4
Mg	7.65	1.334	3.163	13.3
Zn	9.39	1.203	3.532	31

[1] K. J. Schafer, B. Yang, L. F. DiMauro, and K. C. Kulander, Phys. Rev. Lett. **70**, 1599 (1993).
[2] P. B. Corkum, Phys. Rev. Lett. **71**, 1994 (1993).
[3] G. G. Paulus, W. Nicklich, H. Xu, P. Lambropoulos, and H. Walther, Phys. Rev. Lett. **72**, 2851 (1994).
[4] B. Walker, B. Sheehy, L. F. DiMauro, P. Agostini, K. J. Schafer, and K. C. Kulander, Phys. Rev. Lett. **73**, 1227 (1994).
[5] X. F. Li, A. L'Huillier, M. Ferray, L. A. Lompré, and G. Mainfray, Phys. Rev. A **39**, 5751 (1989).
[6] L. V. Keldysh, Sov. Phys. JETP **20**, 1945 (1964).
[7] S. Popruzhenko, J. Phys. B **47**, 204001 (2014).
[8] A. Perelomov, V. Popov, and M. Terent'ev, Sov. Phys. JETP **23**, 924 (1966).
[9] V. S. Popov, Physics-Uspekhi **47**, 855 (2004).
[10] A. Perelomov and V. Popov, Sov. Phys. JETP **25**, 336 (1967).
[11] S. V. Popruzhenko, V. D. Mur, V. S. Popov, and D. Bauer, Phys. Rev. Lett. **101**, 193003 (2008).
[12] S. Chin, F. Yergeau, and P. Lavigne, J. Phys. B **18**, L213 (1985).
[13] M. Ammosov, N. Delone, and V. Krainov, Sov. Phys. JETP **64**, 1191 (1986).
[14] F. Ilkov, J. Decker, and S. Chin, J. Phys. B **25**, 4005 (1992).
[15] V. P. Krainov, J. Opt. Soc. Am. B **14**, 425 (1997).
[16] H. R. Reiss, Phys. Rev. Lett. **101**, 043002 (2008).
[17] S. Augst, D. Strickland, D. D. Meyerhofer, S. L. Chin, and J. H. Eberly, Phys. Rev. Lett. **63**, 2212 (1989).
[18] D. Bauer and P. Mulser, Phys. Rev. A **59**, 569 (1999).
[19] X. M. Tong and C. D. Lin, J. Phys. B **38**, 2593 (2005).
[20] F. H. Faisal, J. Phys. B **6**, L89 (1973).
[21] H. R. Reiss, Phys. Rev. A **22**, 1786 (1980).
[22] K. C. Kulander, Phys. Rev. A **35**, 445 (1987).
[23] J. L. Krause, K. J. Schafer, and K. C. Kulander, Phys. Rev. A **45**, 4998 (1992).
[24] M. J. Nandor, M. A. Walker, L. D. Van Woerkom, and H. G. Muller, Phys. Rev. A **60**, R1771 (1999).
[25] P. Agostini, F. Fabre, G. Mainfray, G. Petite, and N. K. Rahman, Phys. Rev. Lett. **42**, 1127 (1979).
[26] G. Paulus, F. Grasbon, H. Walther, P. Villoresi, M. Nisoli, S. Stagira, E. Priori, and S. De Silvestri, Nature **414**, 182 (2001).
[27] T. Rathje, N. G. Johnson, M. Möller, F. Süßmann, D. Adolph, M. Kübel, R. Kienberger, M. F. Kling, G. Paulus, and A. Sayler, J. Phys. B **45**, 074003 (2012).
[28] P. . M. Paul, E. Toma, P. Breger, G. Mullot, F. Augé, P. Balcou, H. Muller, and P. Agostini, Science **292**, 1689 (2001).
[29] M. Hentschel, R. Kienberger, C. Spielmann, G. A. Reider, N. Milosevic, T. Brabec, P. Corkum, U. Heinzmann, M. Drescher, and F. Krausz, Nature **414**, 509 (2001).
[30] M. Chini, K. Zhao, and Z. Chang, Nature Photon. **8**, 178 (2014).
[31] C. I. Blaga, J. Xu, A. D. DiChiara, E. Sistrunk, K. Zhang, Z. Chen, A.-T. Le, *et al.*, Nature **483**, 194 (2012).
[32] J. Xu, C. I. Blaga, K. Zhang, Y. H. Lai, C. D. Lin, T. A. Miller, P. Agostini, and L. F. DiMauro, Nature Commun. **5** (2014).
[33] M. Pullen, B. Wolter, A.-T. Le, M. Baudisch, M. Hemmer, A. Senftleben, C. D. Schröter, J. Ullrich, R. Moshammer, C.-D. Lin, *et al.*, Nature Commun. **6**, 7262 (2015).
[34] B. Wolter, M. Pullen, A.-T. Le, M. Baudisch, K. Doblhoff-Dier, A. Senftleben, M. Hemmer, C. Schröter, J. Ullrich, T. Pfeifer, *et al.*, Science **354**, 308 (2016).
[35] P. Agostini and G. Petite, J. Phys. B **17**, L811 (1984).
[36] P. Agostini and G. Petite, Journal of Physics B: Atomic and Molecular Physics **18**, L281 (1985).
[37] L. F. DiMauro, D. Kim, M. W. Courtney, and M. Anselment, Phys. Rev. A **38**, 2338 (1988).
[38] G. D. Gillen, M. A. Walker, and L. D. Van Woerkom, Phys. Rev. A **64**, 043413 (2001).
[39] M. Smits, C. A. de Lange, A. Stolow, and D. M. Rayner, Phys. Rev. Lett. **93**, 213003 (2004).
[40] S. M. Hankin, D. M. Villeneuve, P. B. Corkum, and D. M. Rayner, Phys. Rev. A **64**, 013405 (2001).
[41] D. Kielpinski, R. Sang, and I. Litvinyuk, Journal of Physics B: Atomic, Molecular and Optical Physics **47**, 204003 (2014).
[42] M. Pullen, W. Wallace, D. Laban, A. Palmer, G. Hanne, A. Grum-Grzhimailo, K. Bartschat, I. Ivanov, A. Kheifets, D. Wells, *et al.*, Physical Review A **87**, 053411 (2013).
[43] S.-F. Zhao, L. Liu, and X.-X. Zhou, Optics Communications **313**, 74 (2014).
[44] S.-F. Zhao, A.-T. Le, C. Jin, X. Wang, and C. D. Lin, Phys. Rev. A **93**, 023413 (2016).
[45] C. Wang, Y. Tian, S. Luo, W. G. Roeterdink, Y. Yang,

D. Ding, M. Okunishi, G. Prümper, K. Shimada, K. Ueda, and R. Zhu, Phys. Rev. A **90**, 023405 (2014).
[46] K. Zhang, Y. H. Lai, E. Diesen, B. E. Schmidt, C. I. Blaga, J. Xu, T. T. Gorman, F. Légaré, U. Saalmann, P. Agostini, J. M. Rost, and L. F. DiMauro, Phys. Rev. A **93**, 021403 (2016).
[47] W. Wiley and I. H. McLaren, Rev. Sci. Instrum. **26**, 1150 (1955).
[48] A. l'Huillier, L. A. Lompre, G. Mainfray, and C. Manus, Phys. Rev. A **27**, 2503 (1983).
[49] P. B. Corkum, N. H. Burnett, and F. Brunel, Phys. Rev. Lett. **62**, 1259 (1989).
[50] S. Klarsfeld and A. Maquet, Phys. Rev. Lett. **29**, 79 (1972).
[51] T. Nakajima and G. Buica, Phys. Rev. A **74**, 023411 (2006).
[52] X. M. Tong, Z. X. Zhao, and C. D. Lin, Phys. Rev. A **66**, 033402 (2002).
[53] D. Pavičić, K. F. Lee, D. M. Rayner, P. B. Corkum, and D. M. Villeneuve, Phys. Rev. Lett. **98**, 243001 (2007).
[54] I. Thomann, R. Lock, V. Sharma, E. Gagnon, S. T. Pratt, H. C. Kapteyn, M. M. Murnane, and W. Li, J. Phys. Chem. A **112**, 9382 (2008).
[55] H. Li, D. Ray, S. De, I. Znakovskaya, W. Cao, G. Laurent, Z. Wang, M. F. Kling, A. T. Le, and C. L. Cocke, Phys. Rev. A **84**, 043429 (2011).
[56] J. Wu, L. P. H. Schmidt, M. Kunitski, M. Meckel, S. Voss, H. Sann, H. Kim, T. Jahnke, A. Czasch, and R. Dörner, Phys. Rev. Lett. **108**, 183001 (2012).
[57] S.-K. Son and S.-I. Chu, Phys. Rev. A **80**, 011403 (2009).
[58] M. Abu-samha and L. B. Madsen, Phys. Rev. A **80**, 023401 (2009).
[59] S.-F. Zhao, C. Jin, A.-T. Le, T. F. Jiang, and C. D. Lin, Phys. Rev. A **80**, 051402 (2009).
[60] R. Murray, M. Spanner, S. Patchkovskii, and M. Y. Ivanov, Phys. Rev. Lett. **106**, 173001 (2011).
[61] M. Spanner and S. Patchkovskii, Phys. Rev. A **80**, 063411 (2009).
[62] V. P. Majety and A. Scrinzi, Phys. Rev. Lett. **115**, 103002 (2015).
[63] P. Von den Hoff, I. Znakovskaya, S. Zherebtsov, M. F. Kling, and R. de Vivie-Riedle, Applied Physics B: Lasers and Optics **98**, 659 (2010).
[64] I. Barth and O. Smirnova, Phys. Rev. A **87**, 013433 (2013).
[65] S. Augst, D. D. Meyerhofer, D. Strickland, and S.-L. Chin, J. Opt. Soc. Am. B **8**, 858 (1991).